Modeling enantiomeric separations as an interfacial process using amylose tris(3,5- dimethylphenyl carbamate) (ADMPC) polymers coated on amorphous silica

Xiaoyu Wang, ‡ Cynthia J. Jameson, § and Sohail Murad ‡ *

‡Department of Chemical Engineering, Illinois Institute of Technology, 10 West 33rd Street, Perlstein Hall, Chicago, Illinois 60616, United States

§Department of Chemistry, University of Illinois at Chicago, 845 W. Taylor St. Chicago, Illinois 60607, United States

*Corresponding Author e-mail: murad@iit.edu.

ORCID

Xiaoyu Wang http://orcid.org/0000-0003-2228-0114

Cynthia J. Jameson http://orcid.org/0000-0001-5909-0643

Sohail Murad http://orcid.org/0000-0002-1486-0680

Abstract

In the present study, we present a model to predict the chiral separation results for drug enantiomers by ADMPC chiral stationary phase in high performance liquid chromatography (HPLC) wherein multiple ADMPC polymer strands are coated on an amorphous silica slab. Both reactive and classical MD are used to prepare the surface. Using various MD techniques, we successfully coat ADMPCs onto the surface without losing the structural character of the backbone in the presence of the solvent system. Not only is this model more representative of the polymer surface on a solid support that is encountered by the enantiomers, it also provides more opportunities for chiral molecules interacting with ADMPC, resulting in a better agreement compared with experiment when we use overall average quantities as the metric. In our previous studies, we had used a single polymer strand of amylose tris(3,5-dimethylphenyl

carbamate) (ADMPC) in the solvent system. The new model provides the possibility for large drug molecules to interact with two polymer strands at the same instant, which was not possible to model with only a single polymer strand in the solvent. For a better understanding of why some metrics are better predictors than others, we use charts of the distribution of hydrogen bonding lifetimes in this work to display the hydrogen bonding information for various donor-acceptor pairs that contribute to the interaction events determining the relative retention times for the enantiomers. We also examine the contribution of the ring-ring interactions to the molecular recognition process and ultimately to differential retention of S and R enantiomers. The results using the new model are more consistent than the previous models and resolves the problematic case of two drugs, thalidomide and valsartan.

Keywords:

amylose tris(3,5-dimethylphenyl carbamate) (ADMPC), polymers on amorphous silica, chiral separation, high performance liquid chromatography, atomistic molecular dynamics

1. Introduction

In previous work, [1, 2] we have used explicit-solvent fully atomistic molecular dynamics (MD) simulations (permitting all the interactions between the atoms constituting the polymeric chiral stationary phase (CSP), the solvent molecules and the drug molecule) to better understand the chiral recognition mechanism that makes the separation possible. Using amylose tris(3,5-dimethylphenyl carbamate) (ADMPC) as our prototype, three different solvent systems, and ten different racemates as solutes, we

sought to find a molecular dynamics average quantity that could serve as a metric

that predicts which of the two enantiomers will elute first and that also correlates with the ratio of retention times for enantiomers. Several MD average quantities related to hydrogen-bonding lifetimes are found to correlate with the ratio of retention times for the enantiomers. One of these quantities provides a prediction of the correct elution order 90 % of the time, and the ratios of these quantities for the enantiomers provides a correlation (0.85 coefficient) with the experimental separation factor (the ratio of retention times). Nevertheless, this work needs to be improved further for general use, as discussed below.

A single 12-mer strand of the chiral stationary phase may be an insufficient model. We had carried out equivalent studies: one in which the drugs interact with a 12- mer of ADMPC which is freely floating in explicit solvent (Model 1) and another in which the 12-mer is restrained with a weak harmonic potential for each atom of the polymer after equilibration in the solvent (Model 2). The purpose of this restrained polymer study was to discover the extent to which the free movement of all atoms of the short polymer in solution permit greater sampling by donor-acceptor groups. In the case of the restrained polymer, all atoms are still dynamic, but the cavities for “docking” are very regular and consistent in the free volume available to the enantiomers; and this situation may be more typical of very long polymers laid down on the silica support. From the previous work,[1,2] using Model 2, a restrained 12-mer pre-equilibrated in the solvent system appears to be a reasonable model for MD simulations of drug-CSP interactions that form the basis for enantiomeric separation in HPLC where the polymer is coated on the

solid support. The prediction is not perfect, for 10 drugs, we failed to predict which of S or R elutes first in at least one case, with mixed predictions coming from different

metrics in three cases. In one case, while the simulation predicted the correct enantiomer to elute first, there was too great a preference of the polymer for the other enantiomer compared to experiment. Furthermore, with the restrained model, even though the correlation coefficients are close to 0.8, we found the correlation plots were far from a slope of unity, as they would be in an ideal prediction. Thus the need for improved models is obvious.

A third model is one in which only the backbone atoms of the ADMPC 12-mer are restrained, with the atoms of the side chains free to move. In a separate study, we considered Model 3 using the same set of 10 drugs with the ADMPC in their respective solvent systems to find out whether Model 3 could give results that may or may not be improved over Models 1 and 2. Model 3 turned out to be as poor as Model 1; after finishing the simulations for four drugs, benzoin, flavanone, naringenin and valsartan in heptane/isopropyl alcohol (90/10) solvent system, in which all results gave the wrong prediction for the elution order, we abandoned this model.

In the present work, we consider a much more realistic Model 4 which consists of polymer chains on an amorphous silica surface. This model is closer to the experimental conditions. (a) The presence of adjacent polymers is included, thus permitting polymer chain-chain interactions, and also permitting simultaneous interaction of an enantiomer with more than one chain. (b) There is no ad hoc partial restraint on the atomic motions as was used in Models 2 and 3. (c) The atomistic effects

of the silica on the structure and dynamics of the polymer are included. (d) The interaction regions presented by the ADMPC to an enantiomer is limited, permitting approach not from all radial directions from a single chain that is possible with Models 1-

3; rather, approach is only from the face away from the silica. (e) A further improvement is the use of four 18-mer chains instead of a single 12-mer chain. We seek an understanding of the role played by the solid support, and we seek to discover whether Model 4 leads to consistent predictions for which of S or R elutes first, and whether the MD metrics that we have previously developed with the earlier simpler models correlate well enough with experimental separation factors to be used for predicting the magnitudes of the separation factors a priori. We test the Model 4 with 4 sets of enantiomers: benzoin and valsartan in hep/IPA (90/10), and flavanone and thalidomide in methanol.

2. Methods

2.1 Building the model for the amorphous silica

We need a silica slab with a surface area sufficient to accommodate four 18-mer ADMPC chains, and just large enough not to leave uncovered silanols that would interact with the solvent. Our model of the surface of the solid support is based on a model of an amorphous silica interface[3] that captures the essential experimentally known properties. The silica interface comprises two types of groups, silanol and siloxane groups. The siloxane groups are hydrophobic in character, whereas the silanol are hydrophilic. The typical density of silanol groups is 4.6 OH/nm^2. [4, 5] Zhuravlev

provided a detailed description of the chemistry of amorphous silica, defining a maximum number of hydroxyl groups on the surface and categorizing them into subgroups according to their chemical bonding to the surface.[4] Silanol groups are classified as isolated (single silanols), geminal (2 OH groups per Si) and vicinal (bridged

OH groups). [5] Experimentally, according to the Zhuravlev model,[4] they are present in the following surface densities: 1.2, 2.80, and 0.60 OH/nm^2 for isolated, vicinal, and geminal, respectively. The type of silanols, not only their density, determines the hydrophilicity of the silica surface.

2.1.1 Preparation of a starting configuration for the amorphous silica slab Several methods have been used. The GLASSFF force field provided in Cerius2 [6] had been used to generate a starting structure in the original paper that developed the CWCA force field by Schulten et al.[7] A Morse-style potential developed by Demiralp et al. was parameterized to predict phase transitions in ceramics including silica. [8] A well trained ReaxFF, the ReaxFF-Si/SiO/SiN by Fogarty et al. [9] optimized from the original ReaxFF-Si/O/H of van Duin et al.[10] showed good agreement with both experiment and quantum mechanical calculations. A fresh cut structure of amorphous silica slab 7 was used as initial starting configuration and its dimension is 78 × 78 × 15 Å. Then we applied ReaxFF-Si/SiO/SiN by Fogarty et al. [9] to simulate the annealing and quenching processes. We used LAMMPS [11] software package to simulate annealing; a time step of 0.25 fs was used throughout this part. First, an NVE ensemble coupled with Berendsen

thermostat [12] at 300 K was deployed for 50 ps to eliminate initial overlapping atoms and minimize the energy of the system. The first annealing process used Nose-Hoover style non-Hamiltonian NVT ensemble. [13, 14] The system was heated up to 4000 K and gradually cooled down to 300 K at the rate of 25 K/ps. After that, in the second annealing process, the system is heated to 4000 K again using an NPT ensemble, keeping a constant pressure of 1 atm for 75 ps. The barostat was only deployed in the x

and y directions; the z dimension of the simulation box was kept constant, to lead to a thin slab structure at the end. The system is cooled down from 4000 K to 300 K at a rate of 25 K per ps. The above procedure resulted in a silica slab with dimensions of 72.475 × 72.475 × 15 Å.

2.1.2 Preparation of the silanol-capped surface

The silica slab was then submerged into a 72.475 × 72.475 × 45 Å box where the structure was surrounded by water molecules, as shown in Figure 1. Using such a "sandwich" arrangement as in our previous studies,[15,16,17] we increase the contact surface area and thereby facilitate equilibration. ReaxFF-Si/SiO/SiN [9] was applied here which allowed the reactions taking place on the silica surface to cap those dangling silicon and oxygen atoms. An NVT ensemble was used because the difference in compressibility between silica and water could otherwise produce an undesirable structure where silica was surrounded by water in all three directions.

First, a 70 ps simulation was carried out and then the velocities were reassigned according to a temperature 300 K, then final equilibration proceeds for 580 ps. The

above procedure generates a structure of silanol-capped silica which has the right structural information compared with experiments, i.e., a silanol density of 4.72/nm^2 on the surface, which agrees reasonably well with the experimental value of 4.6 /nm, [2, 4, 5] and the distribution of silanol types: 1.26, 2.23, and 1.23 OH/nm^2 for isolated, vicinal, and geminal, respectively, which agrees reasonably well with experimental distribution for isolated and vicinal, although a somewhat higher germinal density. After

equilibration, unreacted water molecules were removed. This silanol-capped silica structure was then used in the following studies.

The so-called CWCA force field incorporating the CHARMM water contact angle Lennard-Jones and bond parameters of Schulten et al.[7] was applied throughout the rest of simulation procedures. A similar model silica surface had been used by Benjamin et al. [18, 19] with a uniform silanol density of 4.62/nm^2; they also used the CWCA force field for MD simulations of binary solvent mixtures (methanol, ethanol, acetonitrile) at the silica surface. Leroch et al. [20] tested several force fields, among them the Clay force field and CWCA for the silica interface with a lower silanol density of 3.0/nm^2 where almost all of the silanol groups are isolated. The set of force field parameters we used (CWCA) are therefore well tested against many experimental quantities as described in these references. Since the number and composition of atoms deviated slightly from the original CWCA paper, the charges on the silicon atoms attached to silanol groups and silanol oxygen and hydrogen are scaled to set the total charge to zero. In order to maintain the bulk silica structure, the bulk atoms were self-tethered throughout the

simulations by applying a harmonic force with a force constant of 500 kcal/mol/Å^2. The parameters are summarized in Table 1.

2.2 Coating the ADMPC on the amorphous silica surface in vacuum First, we constructed 20-mer chains starting from the 12-mer model by Okamoto et al.[21] We characterize the chain backbone structure by mapping the population of the torsional angles, φ: H1-C1-O-C2, ψ: C1-O-C2-H2 in a Ramachandran-like plot, as in our previous work.[1,2] After equilibrating the 20-mer in the particular solvent system for 100

ns, cluster analysis was carried out using the hierarchical agglomerative approach.[22] From the results of the cluster analysis for the backbone atoms, a single representative structure of ADMPC is found in each solvent system (heptane/IPA or methanol). We then remove one monomer from each end and use the 18-mer structure in the following coating process, for the following reasons. The periodic silica base dictates the xy dimensions of the simulation box and we need full coverage by ADMPC of the silanol capped surface. Initially, we started this model development using four 16-mers; however, we found that these polymer fragments were somewhat too short to cover the silanol-capped silica slab, presenting artefactual structural features of the polymer to the enantiomers for polymer end units near the edges. Four 18-mer units would cover the silanol-capped silica slab. In practice, the polymer coated silica should not have any unprotected silanols, otherwise the enantiomers would hydrogen bond to the silanols and cause severe tailing of the HPLC peaks. Also, it is critical to maintain polymer structure and helical properties while coating them onto the silanol-capped silica slab

using van der Waals forces. The industrial process is gradually evaporating the solvent, thus only polymers would be left on the surface eventually. By this way, structural properties of the polymer are ensured as in the solvent atmosphere. In simulations, introducing the polymer strands to the silica in the presence of solvent would permit the solvent molecules to form strong hydrogen-bonds with the silanols on the silica surface, interactions that are far stronger than the van der Waals interactions of the polymer chains to the silica surface. Thus, in simulations, ADMPC polymers in the presence of solvent would never have the chance to stick onto the surface. To prevent this from happening, we developed a multi-step simulation strategy which is explained in more

detail below. Our goal is to explore a way that would leave polymers in solvent-swollen configurations onto the silica slab without leaving exposed silanol groups. Chirality of ADMPC results from the structural chirality of the glucose units, the chirality inherent in the periodic helical grooves in the polymeric backbone. In addition, there is the supramolecular chirality in the regions between adjacent polymer rods, which were not included in previous models 1-3. Since the ADMPC has a handed helical structure (left-handed 4/3 helix), we should consider parallel or antiparallel arrangements of polymer strands, such as those in Fig. 2.

We considered two strategies of interacting the polymer chains with the silica to avoid these problems. In the first, we placed a symmetric parallel arrangement of four chains close to the silica surface without solvent and ran the MD simulation in vacuum. This results in 4 polymer chains van der Waals bonded to the silanol-capped silica slab. (Note that in the absence of solvent, the polymer chains are shorter compared to the

same polymer chain equilibrated in solution in acetonitrile, Hep/IPA, or methanol; the solvent molecules form hydrogen bonds with the CO and NH sites of the polymer, thereby causing the average dynamic structure of the polymer in solution to be swollen compared to that in vacuum.) We then introduced the solvent into the simulation box and ran NVT MD simulations for four periods of 100 ns. To test whether the polymer chains have achieved equilibrium on the silica after the solvent has been introduced, we checked the Ramachandran maps of the (φ, ψ) angle distributions between adjacent glucose units one connection at a time along the entire length of the backbone, for each of the 4 chains; maps were constructed from the last 20 ns of a 100 ns MD simulation. It appears that starting from the dry structure of the polymer on top of the silica slab and

doing an MD run of the swelling process takes much longer time than 400 ns to reach the correct polymer structures. In the process of equilibration; the polymer ends are free to move out as they permit the solvent to intercalate in the grooves. This process continues along toward the middle part of the chain. These units also have to swell, but they are more restricted in their dynamics, since they have connections on both sides that have to be pushed away as the solvent molecules try to intercalate. Therefore, even after 400 ns, while the Ramachandran angle distributions for the end units are in accord with the idealized case, some of the middle units are clearly not. Thus, it is NOT feasible with this procedure to reach the solvent-equilibrated structure of ADMPC polymers on amorphous silica.

We considered a second procedure for arriving more quickly to the equilibrium condition for ADMPC on the silica slab in the presence of solvent: It is more efficient to

lay down polymers that already have the solvent-swollen structure onto the silica surface. Our packing method consists of several steps. First, four arrangements of solvent swollen polymers are created on top of silica slab in the same simulation box without any solvent molecules. We leave enough distance between ADMPC and silica slab (larger than cutoff distance 12 Å). This is achieved by using “Fix Rigid/NVT” at 298 K in LAMMPS [23] to treat the backbone as a rigid system to maintain the solvated inter monomer spacing. In the implementation of the “Fix Rigid/NVT” in LAMMPS, at each time step the total force and torque on each rigid body is computed as the sum of the forces and torques on its constituent particles. The coordinates, velocities, and orientations of the atoms in each body are then updated so that the body moves and rotates as a single entity. We use the equilibrated solvent-swollen average structure for

the 18-mer for each of the 4 chains to be placed with the silica slab for equilibration in vacuum, keeping the backbone rigid, while the side chains are atomistically mobile. The edge atoms at backbone are tethered to each other while keeping a distance of 18 Å, which can make the four strands expand throughout the surface area and forming a seamless membrane to cover the silica surface. The spacing condition along with the “fix/rigid” is applied throughout the packing-in-vacuum processes. Nose-Hoover style non-Hamiltonian NVT ensemble at 298 K with a time step of 0.2 fs and a total of 200,000 steps (40 ps) is used. The polymers are allowed to associate with each other in vacuum without touching the silica surface. It is easier to control the spacing without silica slab because their motions would be restricted by the van der Waals forces when they sit on the surface. Then, a 5 kcal/mole-Å force towards the silica slab is applied to

backbone atoms to force the associated polymers move to the surface. Another 40 ps allows the polymers to associate with the surface (0.2 fs/step, 200,000 steps). At the end, the force toward the silica surface is removed to let the polymer strands adjust their structures (40 ps, 0.2 fs/step, 200,000 steps). In this way, we can preserve the equilibrated solvent-swollen spacing of the backbone groups and permit only the side chain atoms to individually move while equilibrating the polymer strands on the silanol capped amorphous silica slab in vacuum. This equilibration in vacuum was carried out for each of the arrangements shown in Fig. 2. After this equilibration in vacuum, the solvent is introduced.

2.3 Relaxing the ADMPC on the amorphous silica surface in the presence of solvent

Fig. S1 in Supplemental Information shows a sketch of system setup for preparing the solvated ADMPC on amorphous silica. We use PACKMOL[24] to introduce the solvent into the box (in numbers appropriate to have the experimental density and composition). The simulation box size is 72.475 × 72.475 × 90 Å. We placed a bcc wall on the bottom of the box to prevent solvent molecules from interacting with the bottom surface of the silica under periodic boundary conditions. After packing the solvent molecules, we deployed two steps of energy minimization in LAMMPS. First minimization includes solvent atoms only; the second one includes solvent and side chain atoms. Iterations were stopped by one of the four criteria: the tolerance for energy (unitless) is 0.0; the tolerance for force (Kcal/mol-Å) is 1.0×10^{-8}; maximum iteration

number is 1000; maximum number of force/energy evaluations is 100,000. The Polak Ribiere version of the conjugate gradient algorithm was used for minimization.[25] The "fix/rigid" and spacing conditions are kept to run MD simulation for 500 ps (0.5fs/step, 1,000,000 steps). Then the "fix/rigid" is removed for another 500 ps (0.5fs/step, 1,000,000 steps). Finally, the spacing condition is removed for 500 ps (0.5fs/step, 1,000,000 steps). We removed any solvent molecules which were found between the ADMPC and silica surface and packed them back into the bulk solvent region; solvent molecules interact strongly with the silanol groups at the surface, increasing the distance between ADMPC and silica surface, thereby weakening the VDW forces holding the ADMPC to the silica slab, thus permitting the polymer chains to lift off the silica surface.

The next step would be the actual relaxation of ADMPC polymers in the solvent atmosphere. At this stage we switch from LAMMPS to the AMBER software package; [26]

its GPU acceleration feature reduces simulation run times. In AMBER, we carried out three steps, tethering different groups and gradually releasing them. First, the silica, bcc wall and ADMPC chains were tethered by 1000 kcal/mol and we ran MD for 100,000 steps to equilibrate the solvent only. Second, we ran MD for another 100,000 steps with the silica, bcc wall and ADMPC backbone atoms tethered. Third, only the silica and bcc wall were tethered for another 100,000 steps. Then, we increased the joint glucoside dihedrals' energy barriers in the default GAFF library[27] by a factor of 10 and carried out MD simulations for 60 ns with a time step of 2 fs. Finally, the barriers were brought back

to normal and the system of the four 18-mer strands on amorphous silica in the solvent system ran for another 40 ns to equilibrate freely without any constraints. In the case of methanol solvent, we had to take special care to avoid any interactions between the OH and the silanol groups of the underlying silica because these are particularly strong hydrogen-bonding interactions that should not occur if we have complete coverage of silica by the ADMPC. We accomplished this by artificially adjusting the Lennard-Jones parameters specific to these interactions (increasing the distance parameter by factor of 2 and the well depth by a factor of 2 compared to the default GAFF values.

We prepared several equilibrated systems, containing various parallel and antiparallel arrangements of the polymer chains as described in Fig. 2. We tested the completeness of equilibration in each case, shown by the uniformity of the Ramachandran angle distribution plots for each monomer-monomer joint (not shown here), and also by the regularity of the van der Waals surfaces presented by the 4 ADMPC strands on the silanol-capped silica. We carried these out for two solvent

systems: methanol and hep/IPA (90/10). These are the starting system configurations into which the enantiomer molecules will be introduced.

2.4 Interacting the enantiomers with ADMPC on silica

We start the chiral recognition runs with a multi-strand ADMPC on silica, using various combinations of parallel and antiparallel arrangements, each of which has been pre-equilibrated with the silanol-capped silica surface and with solvent, either methanol

or hep/IPA (90/10), before the enantiomers are introduced. We test Model 4 with four racemates: benzoin and valsartan in hep/IPA and flavanone and thalidomide in methanol. We placed 5 molecules of each enantiomer in the simulation box and run 200 ns simulations. (We do this, rather than only a single enantiomer molecule at a time, for efficiency, but we monitored and took steps to minimize stable dimerization of enantiomers, if any.) We carried out these simulations for each of the ADMPC systems whose arrangements are depicted in Fig. 2. We noted any incidences of enantiomer interacting with more than one strand at a time, as well as any incidences of enantiomers sited in inter-strand regions for a succession of time frames. Methods of analysis of hydrogen-bonding lifetimes and the ring-ring interactions between the enantiomers and the ADMPC are used as described in a previous paper.[2] We first analyzed results from each of four arrangements (aaaa), (aabb), (abba), and (abab) individually, to see whether parallel or antiparallel arrangements of the helical polymer strands provide different results for the hydrogen-bonding statistics and the ring-ring interactions. Then, we combined the results together, resulting in equal contributions

from parallel and anti-parallel arrangements, for an overall analysis using the same six MD metrics that we had introduced in previous work. [1, 2]

3. Results and Discussion

3.1 Structural characteristics of ADMPC polymer backbone on amorphous silica

First, we analyze the structures of the polymers equilibrated with the respective

solvents on the silica. Analyzing particular arrangements separately, we ask several questions. (a) Are the Ramachandran-type maps of dihedral angles of the glycoside bond between adjacent monomers (φ, ψ) uniformly similar for every joint between monomers, irrespective of the parallel or antiparallel arrangements? (b) How do these Ramachandran-type maps in Model 4 differ from those found in the same solvent for Model 1 or Model 2? (c) On the basis of (a) and (b), how restrained is the polymer in Model 4 compared to Models 1 and 2? Is this dependent on the parallel/antiparallel arrangement of the polymer strands on the silanol-capped silica? In Fig. S2 in Supplementary Information, we show Ramachandran maps of dihedral angles of the glycoside bond between adjacent monomers of the four 18-mers of ADMPC on silanol capped silica in methanol, for the various parallel/antiparallel arrangements of polymer on the silanol-capped silica. We combine the results for the various parallel/antiparallel arrangements of polymer on the silanol-capped silica equally weighted, producing the over-all combined distribution of backbone structures in Fig. 3. We also compare the backbones of ADMPC in Model 4 with those of Model 1 and Model 2 in Fig. S3.

Examining the distribution of (φ, ψ) torsion angles in the Ramachandran-like plots, we find:

(a) The main finding is that the distribution is confined to the same quadrant in all cases, that is, despite the dynamic structure of the polymer, there is a regularity in the structure of the polymer backbone and this regularity is found in both solvent systems

and (as seen in Fig. S2 in Supplemental Information) for all parallel/antiparallel arrangements on the silica slab. And this regularity is not greatly different from that observed in the single polymer strand in the solvent system. The set of most probable angles is around (φ, ψ) = (-65°, -55°) for the 4 strands on the silica slab in both hep/IPA and in methanol. This is very close to that observed for a single polymer strand in three solvent systems (φ, ψ) = (−60°, −65°). [2]

(b) The distribution varies slightly with the parallel-antiparallel arrangements of four ADMPC strands on the silica slab, more so in methanol than in hep/IPA (as seen in Fig. S2 in Supplemental Information). These differences occur in the low probability angles; the high probability angles remain the same.

(c) The overall distribution of angles for four strands of ADMPC on silica slab, averaged over various parallel/antiparallel arrangements in (a) hep/IPA and (b) methanol solvent systems after equilibration with no constraints seen in Fig. 3 is generally more compact in hep/IPA than in methanol solvent for the four polymer strands on the silica slab averaged over various arrangements. This is different from the single strand of polymer in the solvent system, where the Ramachandran plot shows a more compact distribution in methanol than in hep/IPA [Ref. Paper II]. Nevertheless,

differences occur only in the low probability angles, the high probability angles remain the same.

(d) Comparison of the Ramachandran plots for the present Model 4 with Models 1, 2, and 3 in Fig. S3 in Supplemental Information indicates that indeed, regularity in

backbone structure is observed in all models; the distribution is confined to the same quadrant in all cases with differences that occur primarily in the low probability angles. However, Model 1 appears much more spread out compared to Model 2 or 4, thus presenting, on average, a less regular, less discriminating chiral sites to approaching enantiomers.

3.2 Enantiomer interactions with multi-strand ADMPC polymer surface compared to single ADMPC strand

For a given enantiomer, analyzing particular arrangements separately, we ask several questions. (a) Do the different antiparallel or parallel arrangements of ADMPC on the silica give similar or uniquely different results for hydrogen bonding statistics? (b) Are there any incidences of enantiomers simultaneously interacting with two adjacent polymer strands? (c) Does the probability of such incidences depend on the parallel/antiparallel arrangements of the polymer on the silica?

For a closer view, we show in Fig. 4 the van der Waals surfaces presented by the polymer chains on the silica in the presence of hep/IPA. All four chains have similar grooves to accommodate solvent or the enantiomers, the symmetry of the chains is similar to, but not identical to that found for the free polymer chain in solution. In Fig. 4, we compare a polymer chain in Model 4 with (a) the perfect Okamoto structure, and (b)

the single polymer strand in the solvent. This Model 4 is closer to the practical system than any other models that have been considered previously.

An earlier study by Li et al. of ADMPC on silica gel in vacuum (no solvent) used a

silica gel model in which silanol groups are fully end-capped with aminopropyl silane and a 13-mer ADMPC segment selected from a 36-mer equilibrated in vacuum by choosing the segment with the greatest number of chiral cavities compared with other segments that were not selected. [28] They fixed the backbone dihedral angles (φ, ψ) at exactly (-68.5°, -42.01°), the same as reported for ADMPC in solution in $CHCl_3$ by Yamamoto. [21] Docking simulations were carried out by these authors in vacuum, with rigid enantiomers and rigid ADMPC. In contrast, our Model 4 (a) incorporates the solvent system, (b) includes more than one polymer chain, thus permitting chain-chain interactions as well as permitting an enantiomer to interact with 2 (or more) chains simultaneously. Furthermore, in the present work, our MD simulations of the interactions of enantiomers with the ADMPC on the silica are fully atomistic and fully dynamic, occurring without any restraints of any kind, and equilibrated with solvent.

Incidences of an enantiomer hydrogen-bonded to two ADMPC chains simultaneously are observed in the case of valsartan. We show in Fig. 5 a few snapshots demonstrating this phenomenon. Although such incidences do not dominate the overall results, only Model 4 can permit such occurrences to be included; single strand models of Models 1-3 miss these events entirely. In the examples shown in Fig. 5, the close interactions with two adjacent strands involve hydrophobic interactions with one strand, simultaneously with hydrogen bonding to the other strand.

Antiparallel or parallel arrangements of polymer chains on the silica do not provide very different results for benzoin or flavanone. This is probably the case because the

incidences of enantiomers having long-lived associations with two adjacent chains simultaneously are not observed for benzoin or flavanone. Since the enantiomer has long-lived interactions with only one polymer at a time, it is relatively unaware of the distinction of the adjacent chain being parallel or antiparallel relative to the one that it is hydrogen-bonded to. Only in the case of valsartan did we observe the enantiomer interacting with two polymer strands simultaneously, as seen in the snapshots in Fig. 5.

3.3 Analysis of hydrogen bonding lifetimes

The distribution of hydrogen bonding lifetimes for benzoin are shown in Fig. 6 for R and S enantiomers in hep/IPA interacting with the ADMPC on silica. This constitutes the combined results for all arrangements of the polymer strands on the silica.

The distributions of lifetimes of hydrogen bonds between various donor-acceptor pairs are markedly different for the S and R enantiomers of benzoin in hep/IPA, with the S enantiomer having consistently many more incidences of longer lifetimes compared to R, for each of the donor-acceptor pairs, as seen in Fig. 6. In this distribution display, we can spot the donor-acceptor pair that provides the longest lifetime that provides the metric called Max Max LT. Given the dynamic nature of the interaction between benzoin enantiomers and the ADMPC shown by the distribution of hydrogen-bonding lifetimes, we note that this specific metric alone, particularly for benzoin, cannot possibly provide the correct overall prediction. The tall bars correspond to lifetimes that contribute the most to Avg LT for each donor-acceptor pair. From the distributions seen in Fig. 6, we

can already infer that S-benzoin elutes last, in agreement with experiment (Ref. 2),

without carrying out the averages over the lifetimes. Each of the four individual arrangements of parallel and anti-parallel strands also provide the same inference, as can be seen in Fig. S5 in Supplemental Information, although the actual distributions are different. *For each arrangement*, comparing individual hydrogen-bonding partners, the lifetime distributions clearly indicate that the lifetimes for the S-benzoin are collectively longer than for the R enantiomer. This seems to indicate that the inter-strand structure does not play a very important role in the hydrogen-bonding between the enantiomers and the ADMPC sites.

From the distributions seen in Fig. 7 for flavanone in methanol, we can likewise easily infer that S elutes last, in agreement with experiment (Ref. 1), even before carrying out the averaging that leads to Overall AvgLT. Although in this particular example, Max MaxLT would give the same conclusion, the latter metric ignores all the dynamic information contained in the entire distribution of hydrogen-bonding lifetimes available in Fig. 7.

Distributions for two other drugs (thalidomide in methanol and valsartan in hep/IPA) are shown in Fig. S6 and S7 respectively, in the Supplemental Information. For thalidomide in methanol the distributions of lifetimes in Fig. S6 clearly show longer lifetimes for the R relative to the S enantiomer, consistently for most of the donor acceptor pairs. For valsartan in hep/IPA the distributions of lifetimes in Fig. S7 clearly show longer lifetimes for the S relative to the R enantiomer, although some donor acceptor pairs are dominant for S, others for R. The distribution plots show that choosing MaxLT as a leading source of MD metrics is misguided. We find that plots of

the distribution of hydrogen-bonding lifetimes over four (because we do all 4 arrangements independently) 200 ns MD simulation runs (in which we observe the full all-atom atomistic dynamics of 5 molecules of each enantiomer interacting with four 18-mer strands of ADMPC polymer on silanol-capped silica slab) is a useful representation of this important aspect of the dynamic chiral recognition process that occurs between the enantiomers and the polymers on the silica.

In our previous work using Model 2, we summarized the hydrogen-bonding lifetime observations in a table listing the dominant hydrogen-bonding interactions for enantiomers with a single slightly restrained ADMPC polymer in solution, naming the individual donor-acceptor pairs and stating whether longer lived for R or for S for each donor-acceptor pair. Clearly, the plots shown in Fig. 6 and 7, and Fig. S6 and S7 are a superior quantitative version of this type of information, leading to a prediction of which of R or S elutes first. Now, we can compare with Table 2 in Ref. 2 for the four drug compounds we studied here to see whether Model 2 gives the same result for each donor-acceptor pair as the more complete Model 4 that has several ADMPC polymers on an amorphous silica slab. The prediction of which enantiomer of benzoin elutes first in hep/IPA solvent in Model 2 is the same as that found here. In both models, the $C{=}O_{drug}$ - HN_{csp} is longer-lived for the S enantiomer, as is the OH_{drug} - $O{=}C_{csp}$, and the R is slightly favored for the $O(H)_{drug}$ - HN_{csp}. For flavanone in methanol, the $C{=}O_{drug}$ - HN_{csp} pair is dominant for both models, both giving S as having the longer-lived hydrogen bonds. Thus, for both the benzoin enantiomers in hep/IPA, and the flavanone enantiomers in methanol, Model 2 seems to have done as well as the present model.

However, for thalidomide and valsartan, Model 2 did not do as well as the present Model. In thalidomide, O1 and O4 are the C=O in the dioxopiperidine portion of the molecule, O4 being the one para to the chiral center. O3 and O2 are the C=O in the isoindoline 1,3 dione part of the molecule; O3 is on the less crowded side. In the case of thalidomide, Model 2 identified NH_{drug} - $O=C_{csp}$ and $C=O1_{drug}$ - HN_{csp} as two donor acceptor pairs that are dominantly longer lived for S only (negligible for R), while $C=O3_{drug}$ - HN_{csp} is dominant and long-lived for R only, and both R and S participate in $C=O4_{drug}$ - HN_{csp}, longer-lived for R. On the other hand, Model 4 finds for S enantiomer the pairs NH_{drug} – $O=C_{csp}$, $C=O1_{drug}$ - HN_{csp}, $C=O4_{drug}$ - HN_{csp}, (just as in Model 2) having the longest lived hydrogen bonds in decreasing order, with $C=O2_{drug}$ - HN_{csp} making some contribution. For the R enantiomer, Model 4 finds the 3 most long-lived hydrogen bonds in the order NH_{drug} – $O=C_{csp}$, $C=O1_{drug}$ - HN_{csp}, (*both missed by Model 2*), followed by $C=O4_{drug}$ - HN_{csp}, and $C=O3_{drug}$ - HN_{csp} (both also found by Model 2). It is quite clear that having missed two leading contributions to hydrogen bonding partners for the R enantiomer, it would be difficult for Model 2 to arrive at the correct answer that S thalidomide elutes first, found experimentally. [29] In the case of thalidomide, a model that includes having polymer strands on the amorphous silica surface appears to be necessary; Model 2 was insufficient.

The case of valsartan is an interesting one. Model 2 did predict that R elutes first, having found S enantiomers forming many long-lived hydrogen bonds in 5 donor acceptor pairs; the incidences of R enantiomers forming hydrogen bonds were far

fewer, leading to a ratio of S/R orders of magnitude larger than the experimental separation factor of 1.29 reported by us in Ref. **2**. In the case of valsartan, Model 4

does reveal the large number of donor-acceptor pairs involved in hydrogen bonds between enantiomer and ADMPC that Model 2 had found, as well as several others that were not found by Model 2. Model 4 provides a more complete sampling for both enantiomers, by a factor:

4 strands x (16/10) mers excluding ends x 5 molecules x 4 arrangements x 200/300 ns = 85.3.

Furthermore, by providing the possibility of the valsartan molecule interacting with more than one strand at the same time, as seen in the examples shown in Fig. 5 (not available in Model 2), and eliminating approaches from all directions around a polymer strand that are possible in Model 2, Model 4 captures the mode of interaction of valsartan with ADMPC on amorphous silica surface in hep/IPA in a more realistic way than was possible with Model 2. For this molecule this appears to make a big difference; and we expect this also to be the case with larger drug molecules.

In Table 2 we provide the results using the same MD metrics as was introduced in our previous work. These results are based on a combination of results from the four parallel/antiparallel arrangements in Fig. 2; the sum of the 4 different arrangements represents parallel and antiparallel grooves equally. The results are more consistent between metrics than Model 2, possibly because of the 85 times as many opportunities for an enantiomer to interact with the polymer in the current results. It is still true that different metrics give different results, but, at least in the case of benzoin and flavanone, Model 4 provides better consistency across all metrics as to which enantiomer elutes

first. This may be due to the fewer number of possible donor-acceptor pairs compared to thalidomide and valsartan; the results for the latter could still be improved by longer MD runs. For thalidomide only the Avg of MaxLT and the Overall Average LT provide

the correct elution order. On the other hand, using Model 2 these two metrics actually gave the wrong elution order. In the case of valsartan, the S/R ratios are more reasonable in the present work, no longer the 14-4600 found by Model 2. This is possibly due to better statistics in the present study, whereas with Model 2 the R enantiomer had extremely few hydrogen bonding events. Even more important may be the structure of Model 4 being more realistic, providing multiple strands which we observed to be important for valsartan. Finally, the overall average hydrogen-bonding lifetime appears to be the best MD metric.

3.4 The role of ring-ring interactions

Next, we examine the interactions between the rings on the benzoin enantiomers with the dimethylphenyl ring on the ADMPC for various parallel/antiparallel arrangements of the polymers on the amorphous silica slab. Comparing these plots, we find that the interaction of benzoin with Model 4 ADMPC is independent of the parallel/antiparallel arrangements. The ring-ring interactions for benzoin with ADMPC polymers on silica are shown in Fig. 8 The corresponding plots for the individual arrangements (aaaa, aabb, abba, abab) are shown in Fig. S8 in Supplementary Information; the sum over all arrangements weighted equally is in Fig. 8.

The interactions of the polymer chains with the amorphous silica maintains the polymer

configuration relatively restrained. This can be seen in Fig. 8, with rather sharp highly probable (γ,θ) distributions in the vicinity of (10°,30°) in the interactions of benzoin rings with the closest ADMPC ring. In this sense, Model 4 is quite similar to Model 2. (The corresponding figure for Model 2 is given in the previous paper.) [2] In both Models

4 and 2, there is an observed preference for average angles in the vicinity of γ = 10°, θ = 30° for both rings in benzoin and the ADMPC rings. Furthermore, Fig. 8 shows a difference between the ring-ring interaction maps for the S and the R enantiomers. This indicates that the Model 4 of the ADMPC on the silica surface presents to the S and R enantiomers of benzoin a chiral-selective restrained (via its interactions with the silica surface) polymer. It appears that the nature of this restraint is approximated to some extent by that which we imposed artificially on a single polymer strand in solution in Model 2. We find differences between the various combinations of parallel and antiparallel arrangements in Fig. S8 in the maps of the angles for the individual arrangements (aaaa), (aabb), (abba) and (abab); yet all of them exhibit the same highly populated regions (γ, θ) = 10-15°,30-40° for both rings in benzoin and the ADMPC rings. Differences show up in the less populated regions from one arrangement to another, and distinct differences between S and R are found in every arrangement. In Fig. 8 we see that there is a distinction between R and S angle distributions of the orientation of the benzoin rings with the rings of ADMPC, just as we had found in similar analysis using Model 2. This is a clear indication, as we had indicated in our previous work based on Model 2, that the ring-ring interactions play an important role in the chiral discrimination, although not in the form of attractive face-to-face or displaced parallel

configurations as originally proposed in static models. As we had previously pointed out, those canonical forms of planar ring-ring orientations are not found in the distribution of angles that are observed in the MD simulations. The present results retain those earlier conclusions.

In contrast, the (γ,θ) angle distributions using Model 1 (a free-floating ADMPC polymer strand in solution) are shown in Fig. S9; the most probable (γ,θ) angle values are much more spread out. Even more important is that, for Model 1, the plots are almost indistinguishable for the S vs. R enantiomers, an indication of the lower chiral selectivity of the Model 1 ADMPC, in hindsight a good reason for giving up the model in earlier work.

4. Conclusions

We have prepared a physical model (Model 4) that is closer to the real chiral stationary phase system where ADMPC is coated on amorphous silica and is equilibrated in the solvent system. We took special care in approaching the final model of ADMPC on amorphous silica in the solvent system so as to reach the correct polymer structure in the presence of both the amorphous silica and the solvent. Clearly, equilibrating the polymer strands with the amorphous silica in vacuum and then exposing the system to solvent is not the way to go since it would take an unfeasible very long MD run before the polymer strands could come to equilibrium with both silica and solvent. This we proved by examining the evolution of the individual monomer-to

monomer glycosidic angles of the backbone in a series of MD runs; we never reached the point where the backbone structure became equilibrated. The resulting model is a distinct improvement over Model 2 which was a slightly restrained single polymer strand in solution. The new model provides the possibility of an enantiomer interacting simultaneously with two polymer strands on the surface, occurrences that any model using a single polymer strand of any length cannot provide. We have observed such

events for valsartan in hep/IPA, but not for benzoin, flavanone, or thalidomide. This may be due to the latter molecules being more compact and able to interact with only one polymer strand at a time. The results show that different parallel and anti-parallel arrangements of the polymer strands retain the conclusions of the sum of the results over all 4 arrangements. The ring-ring interactions for benzoin interacting with Model 4 ADMPC are very similar to what we observed in Model 2, providing a discrimination between S and R enantiomers. While the simpler cases of benzoin and flavanone (few donor-acceptor pairs between enantiomer and ADMPC) did not reveal the weaknesses of Model 2 with respect to the prediction of elution order, thalidomide and valsartan enantiomers were problematic in our earlier work. The present model gives a more complete accounting of the hydrogen bonding lifetimes in various donor-acceptor pairs for thalidomide, thus leading to an unequivocal prediction that S elutes first, whereas Model 2 gave mixed results with various metrics. The present model also provides a more conclusive result for which metrics are superior predictors compared to the others. The new results show that using an overall average of the hydrogen-bonding lifetimes, rather than maximum values of lifetimes for various donor-acceptor pairs gives more consistent results. The case of valsartan is also resolved, leading to not only the correct

elution order (R elutes first, just as predicted using Model 2) but a more reasonable value for the S/R ratio which compares favorably with the experimental separation factor. Future work involving the same chiral stationary phase with the same solvent system is straightforward, since we have derived the starting configuration for each of 4 parallel and antiparallel arrangements and MD runs can be carried out upon introduction

of the enantiomers into the simulation box. The procedural protocol we have developed can be used with other combinations of chiral stationary phases and solvent systems.

Tables and Figures

Table 1. Parameters used for silanol-capped amorphous silica

Non-bonded interactions	ε kcal/mole	σ Å	e q
Si (bulk)	0.300	3.825	0.9000
O_b (bulk)	0.150	3.118	-0.4500
Si (silanol)	0.300	3.825	0.9021
O_h (silanol)	0.300	3.118	-0.6579
H_h (silanol)	0.046	0.713	0.4321

Bonds	K_b kcal/mole	R_0 Å
Si-O_b	885.10	1.61
Si-O_h	428.00	1.61
O_h-H_h	554.13	1.0

Angles	K_a kcal/(mole rad^2)	r_0 degree
O_b−Si−O_h	153.26	111.09
O_h-Si-O_h	89.62	116.26
Si-O_h-H_h	57.50	106.0

Table 2. Comparison of various possible metrics (MD quantities) for Model 4 that may be correlated with experimental ratios of residence times for the enantiomers with ADMPC in the solvent system. S/R ratios, for each metric are given. Values less than 1.00 (corresponding to S elutes first) are in red.

Racemate	Solvent	S/R ratio of various quantities						Expt S/R	Expt elutes first	Predict Order?
		Max of HBframes	Max of MaxLT	Max of AvgLT	Avg of HBframes	Avg of MaxLT	Overall AvgLT			
benzoin	Hep/IPA	1.64	1.15	1.60	1.13	1.78	2.20	1.25 [a]	R [a]	yes
flavanone	MeOH	3.80	1.26	1.84	3.73	1.62	1.79	2.52 [a]	R [b]	yes
thalidomide	MeOH	2.12	1.02	1.58	2.70	0.50	0.59	0.47 [c] 0.35 [d] 0.77 [e]	S [e]	yes from avg
valsartan	Hep/IPA	4.48	0.52	1.79	1.00	1.16	2.00	1.29 [a]	R [a]	yes

[a] Experimental separation factors and elution orders were previously reported in Ref. 2.

[b] α = 2.17 for flavanone in methanol, with the (*R*)-(+) enantiomer eluted as the first

peak, from Ref. 30.

[c] Ref. 31

[d] α = 2.89 for thalidomide in methanol, from Ref. 32.

[e] α = 1.30 for thalidomide in methanol, with the (*S*)-(-) enantiomer eluted as the first peak, from Ref. 29.

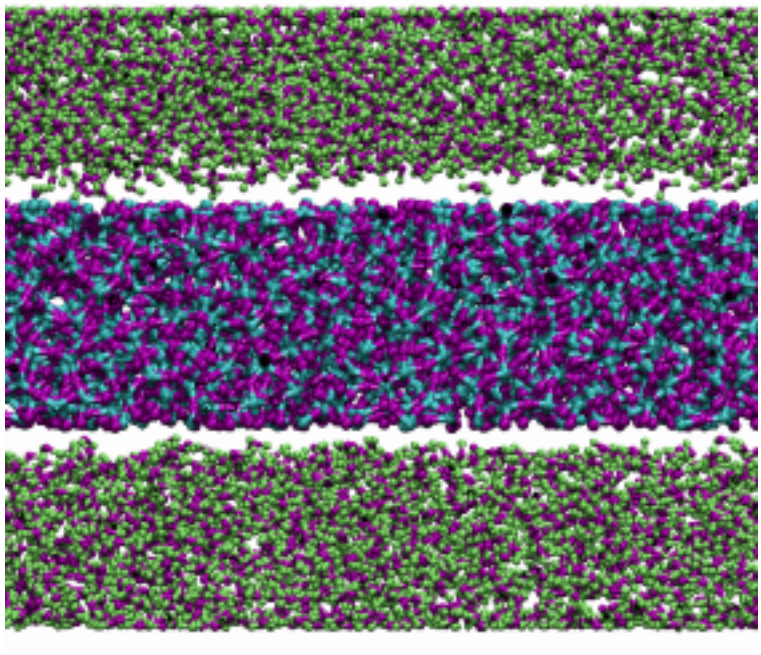

Figure 1. System setup for preparation of silanol-capped surface in which the silica slab in the center is exposed to water regions on both sides. Rectangular volumes of water were generated from a pre-equilibrated water box.

Figure 2. Different arrangements of 18-mer ADMPC strands on silica surface: (a) aaaa; (b) aabb; (c) abba, (d) abab. Neglecting the edges, each arrangement provides some number of inter-strand grooves arising from parallel and antiparallel strands, respectively (4,0), (2,2), (2,2), (0,4), considering periodic boundary conditions. Taken altogether, they result in an equal number (8) of each.

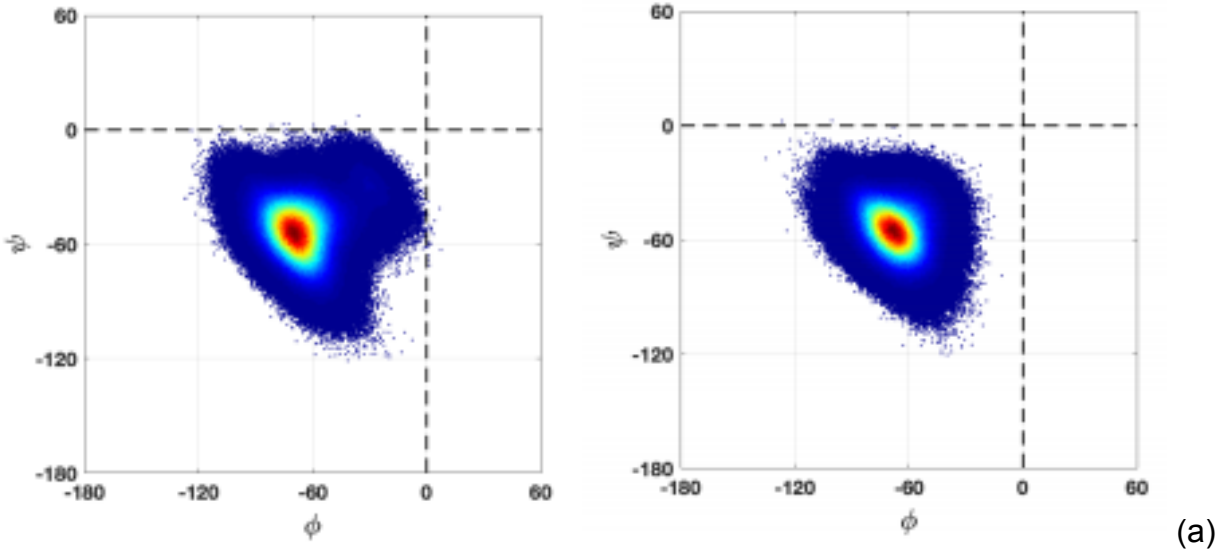

(a)

Figure 3. Distribution of angles for four strands of ADMPC on silica slab, averaged over various parallel/antiparallel arrangements in (a) in hep/IPA (90/10) (b) in methanol

hep/IPA and (b) methanol solvent systems after equilibration with no constraints.

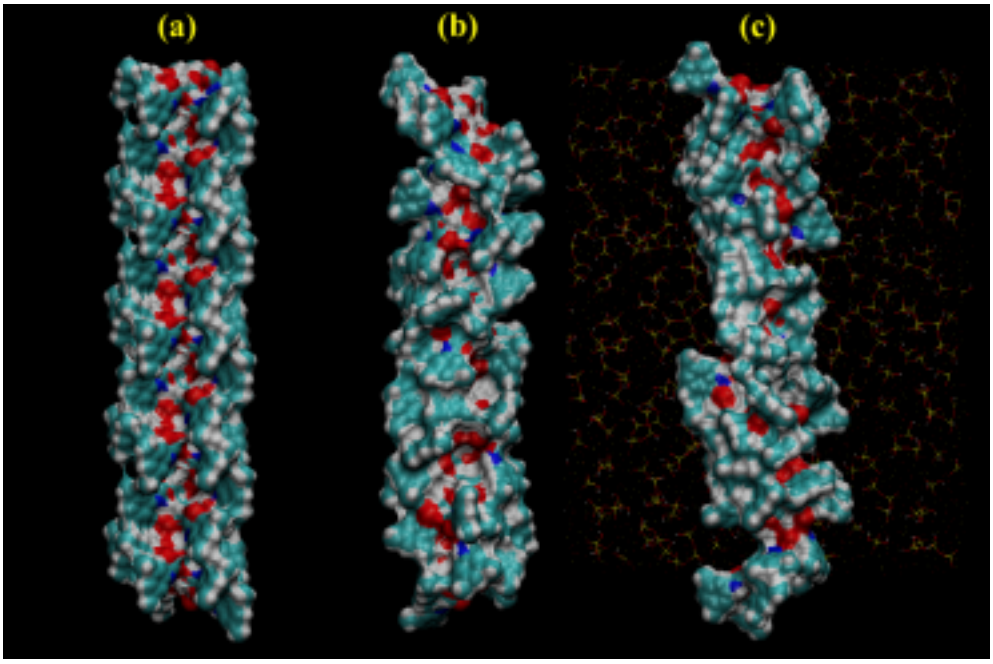

Figure 4. The van der Waals surface presented by a polymer chain (a) in the perfect Okamoto structure, (b) for a single snapshot in the polymer chain in solvent hep/IPA, (c) for a single snapshot of one of four chains in parallel (aaaa) arrangement on the silanol capped silica in the presence of hep/IPA, showing only one chain for clarity.

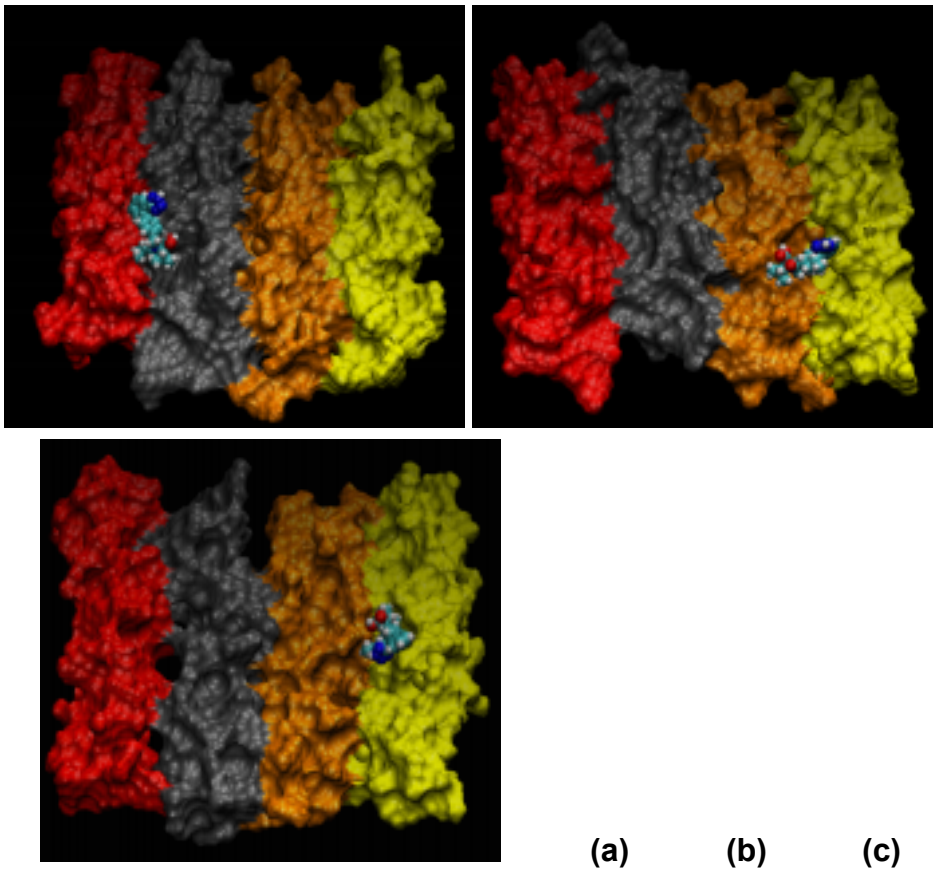

(a) **(b)** **(c)**

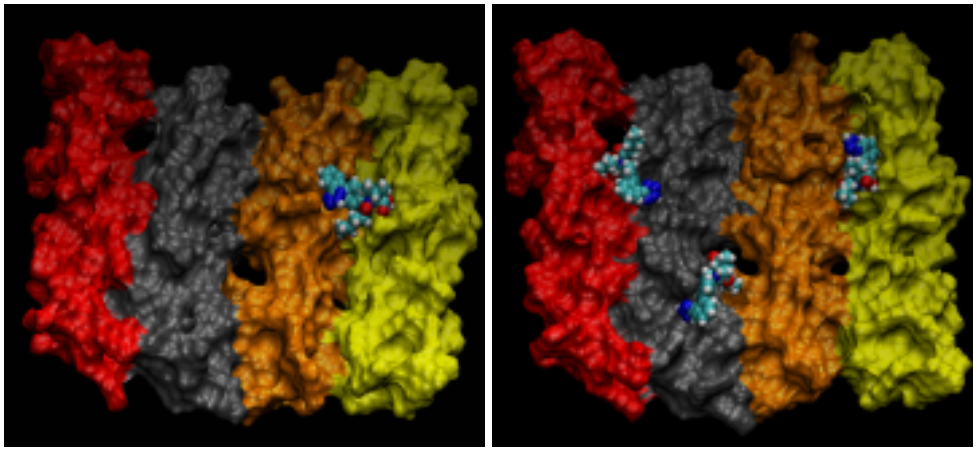

(d) (e)

Figure 5. Snapshots from MD simulations in which incidences of valsartan interacting with two adjacent polymer strands were observed to persist for several frames. (a) R enantiomer on aaaa arrangement of ADMPC on amorphous silica, (b) S on abab, (c) R on abba, (d) S on aabb, (e) three S enantiomers on aabb.

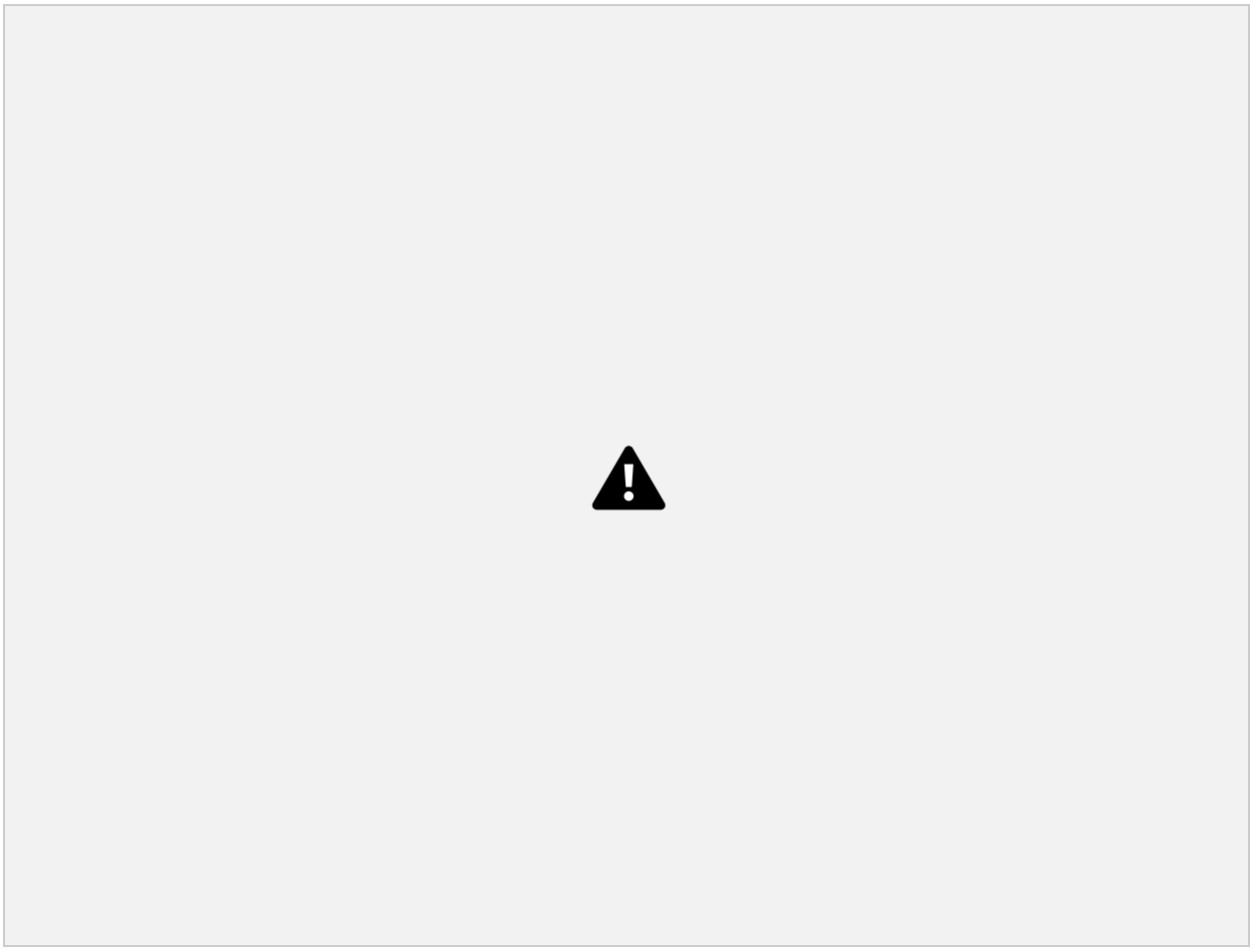

Figure 6. Distribution of lifetimes of hydrogen bonds between R or S enantiomers of benzoin and ADMPC on silica in hep/IPA.

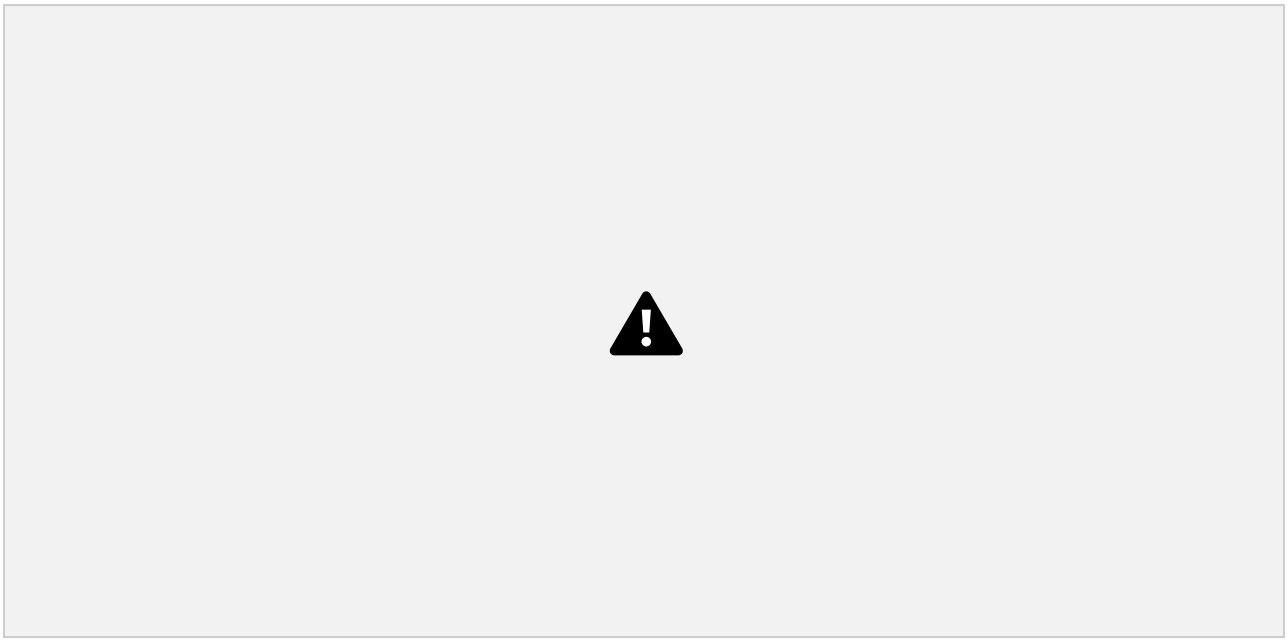

Figure 7. Distribution of lifetimes of hydrogen bonds between R or S enantiomers of flavanone and ADMPC on silica in methanol.

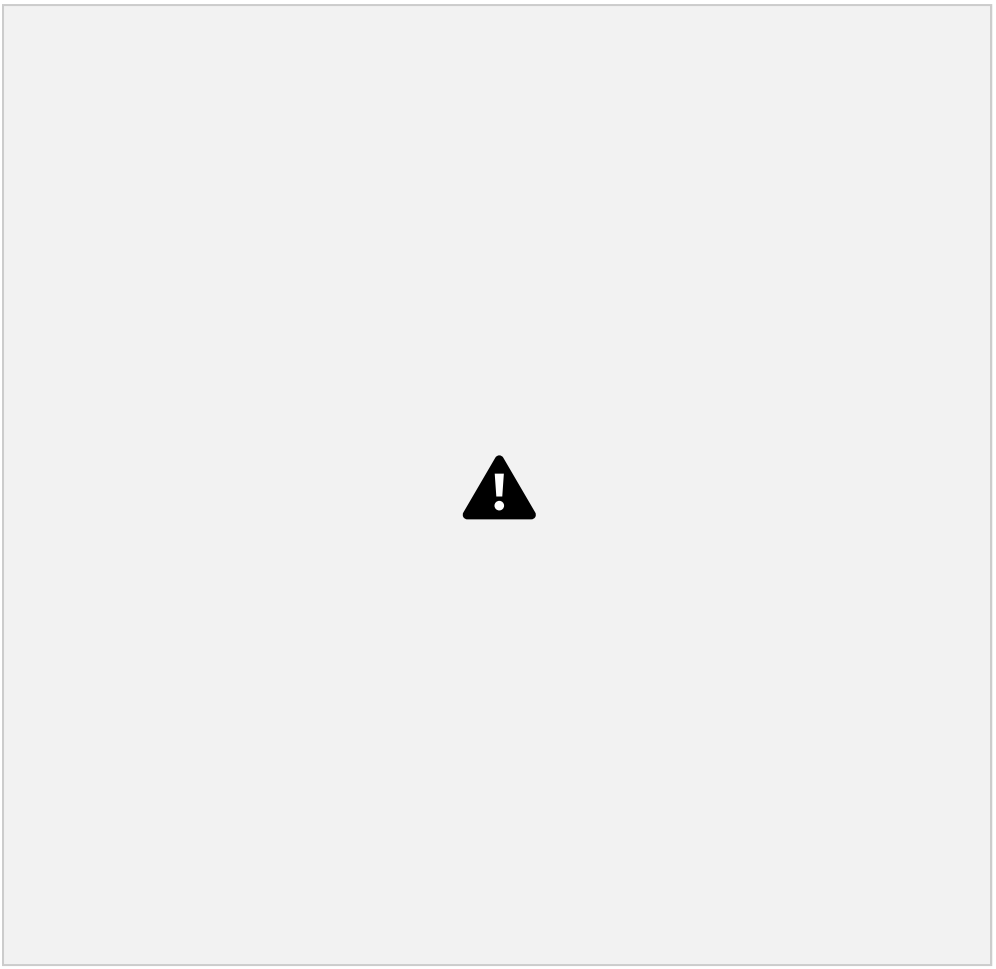
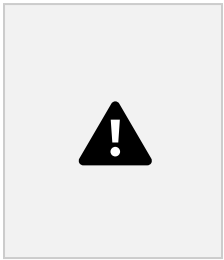


Figure 8. Map of the angles describing the distribution of relative orientations of the phenyl rings (γ = vertical axis, θ= horizontal axis), found for distances R_{cen} less than 4.4 Å between the center of the phenyl ring#1 and ring#2 of the benzoin molecule and the closest ADMPC phenyl ring, using Model 4 in heptane/isopropanol. The colors from blue to red represent the density of the data points going from low to high. The results are based on snapshots uniformly taken from a 100 ns trajectory, (a) for the R enantiomer (b) for the S enantiomer for ring #1, (c) for the R enantiomer (d) for the S enantiomer for ring #2 for each of the various arrangements.

The authors declare no competing financial interest.

ACKNOWLEDGMENTS

This work was supported by The National Science Foundation (CBET 1545560). We thank Professor Ayappa from Indian Institute of Science for suggesting that we display

the distributions of hydrogen bonding lifetimes.

REFERENCES

[1] Zhao, B.; Oroskar, P. A.; Wang, X.; House, D.; Oroskar, A.; Oroskar, A.; Jameson, C. J.; Murad, S. The Composition of the Mobile Phase Affects the Dynamic Chiral Recognition of Drug Molecules by the Chiral Stationary Phase. *Langmuir* **2017,** *33* (42), 11246-11256.

[2] Wang, X.; House, D.; Oroskar, A.; Oroskar, A.; Jameson, C. J.; Murad S. Molecular Dynamics Simulations of the Chiral Recognition Mechanism for a Polysaccharide Chiral Stationary Phase in Enantiomeric Chromatographic Separations. *Mol. Phys*. **2019**, *xx*, xxx-xxx. DOI: 10.1080/00268976.2019.1647360

[3] Lorenz, C. D.; Crozier, P. S.; Anderson, J. A.; Travesset, A. Molecular Dynamics of Ionic Transport and Electrokinetic Effects in Realistic Silica Channels. *J. Phys. Chem. C* **2008**, *112*, 10222–10232. DOI: 10.1021/jp711510k

[4] Zhuravlev, L. T. The surface chemistry of amorphous silica. Zhuravlev model. *Colloids Surf. A.* **2000**, *173*, 1-38. DOI: 10.1016/S0927-7757(00)00556-2

[5] Iler, R. K. The Chemistry of Silica: Solubility, Polymerization, Colloid and Surface Properties and Biochemistry of Silica, Wiley: New York, **1979**. ISBN: 978-0-471-02404-0

[6] Cerius2, v.4.9, Accelrys, Inc. 2003.

[7] Cruz-Chu, E. R.; Aksimentiev, A.; Schulten, K. Water−Silica Force Field for Simulating Nanodevices. *J. Phys. Chem. B* **2006**, *110*, 43, 21497-21508. DOI: 10.1021/jp063896o

[8] Demiralp, E.; Çağin, T.; Goddard, W. A. Morse Stretch Potential Charge Equilibrium Force Field for Ceramics: Application to the Quartz-Stishovite Phase Transition and to Silica Glass. *Phys. Rev. Lett.* **1999,** *82* (8), 1708-1711.

[9] Fogarty, J. C.; Aktulga, H. M.; Grama, A. Y.; van Duin, A. C. T.; Pandit, S. A. A Reactive Molecular Dynamics Simulation of the Silica-Water Interface. *J. Chem. Phys.* **2010,** *132*, 174704. DOI: 10.1063/1.3407433

[10] van Duin, A. C. T.; Strachan, A.; Stewman, S.; Zhang, Q.; Xu, X.; Goddard, W. A., ReaxFFSiO Reactive Force Field for Silicon and Silicon Oxide Systems. *The J. Phy. Chem. A* **2003,** *107* (19), 3803-3811.

[11] Plimpton, S. Fast Parallel Algorithms for Short-Range Molecular Dynamics, J Comp Phys, **1995**, *117*, 1-19. https://lammps.sandia.gov/

[12] Berendsen, H. J. C.; Postma, J. P. M.; Gunsteren, W. F. v.; DiNola, A.; Haak, J. R. Molecular Dynamics with Coupling to an External Bath. *J. Chem. Phys*. **1984**,

81 (8), 3684-3690.
[13] Nosé, S. A Unified Formulation of the Constant Temperature Molecular Dynamics Methods. *J. Chem. Phys*. **1984**, *81* (1), 511-519.
[14] Hoover, W. G. Canonical Dynamics: Equilibrium Phase-Space Distributions. *Phys. Rev. A* **1985**, *31* (3), 1695-1697.
[15] Qu, F.; Shi, R.; Peng, L.; Zhang, Y.; Gu, X.; Wang, X.; Murad, S., Understanding the Effect of Zeolite Crystal Expansion/Contraction on Separation Performance of NaA Zeolite Membrane: A Combined Experimental and Molecular Simulation Study. *J. Membrane Sci.* **2017,** *539*, 14-23.
[16] Wang, X.; Gu, X.; Murad, S., Molecular dynamics simulations of liquid-liquid phase equilibrium of ternary methanol/water/hydrocarbon mixtures. *Fluid Phase Equilibria* **2018**, *470*, 109-119.
[17] Hinkle, K.; Wang, X.; Gu, X.; Jameson, C. J.; Murad, S., Computational Molecular Modeling of Transport Processes in Nanoporous Membranes. *Processes* **2018,** *6* (8), 124. https://doi.org/10.3390/pr6080124
[18] Karnes, J. J.; Benjamin, I. Mechanism and Dynamics of Molecular Exchange at the Silica/Binary Solvent Mixtures Interface. *J. Phys. Chem. A* **2015**, *119*, 12073−12081 DOI: 10.1021/acs.jpca.5b05097
[19] Karnes, J. J.; Gobrogge, E. A.; Walker, R. A.; Benjamin, I. Unusual Structure and Dynamics at Silica/Methanol and Silica/ Ethanol Interfaces. A Molecular Dynamics and Nonlinear Optical Study. *J. Phys. Chem. B* **2016**, *120*, 1569−1578, DOI: 10.1021/acs.jpcb.5b07777
[20] Leroch, S.; Wendland, M. Simulation of Forces between Humid Amorphous Silica Surfaces: A Comparison of Empirical Atomistic Force Fields. *J. Phys. Chem. C* **2012**, *116,* 26247−26261. DOI: 10.1021/jp302428b
[21] Yamamoto, C.; Yashima, E.; Okamoto, Y., Structural Analysis of Amylose Tris(3,5-dimethylphenylcarbamate) by NMR Relevant to Its Chiral Recognition Mechanism in HPLC. *J. Am. Chem. Soc.* **2002,** *124* (42), 12583-12589.
[22] Shenkin, P. S.; Mcdonald, D. Q. Cluster Analysis of Molecular Conformations. *J. Comput. Chem*. **1994**, *15*, 899-916.
[23] https://lammps.sandia.gov/doc/fix_rigid.html
[24] Martínez, L.; Andrade, R.; Birgin, E. G.; Martínez, J. M., PACKMOL: a package for building initial configurations for molecular dynamics simulations. J. Comput. Chem. **2009**, *30*(13), 2157-2164.
[25] Polak, E.; Ribiere, G., Note sur la convergence de méthodes de directions conjuguées. *Rev. Fr. Inform. Rech. Oper.* **1969,** *3* (1), 35-43. http://www.numdam.org/item?id=M2AN_1969__3_1_35_0
[26] Case, D. A.; Babin, V.; Berryman, J. T.; Betz, R. M.; Cai, Q.; Cerutti, D. S.; Cheatham, T. E.; Darden, T. A.; Duke, R. E.; Gohlke, H.; Goetz, A. W.; Gusarov,

S.; Homeyer, N.; Janowski, P.; Kaus, J.; Kolossváry, I.; Kovalenko, A.; Lee, T. S.; LeGrand, S.; Luchko, T.; Luo, R.; Madej, B.; Merz, K. M.; Paesani, F.; Roe, D. R.; Roitberg, A.; Sagui, C.; Salomon-Ferrer, R.; Seabra, G.; Simmerling, C. L.; Smith,

W.; Swails, J.; Walker; Wang, J.; Wolf, R. M.; Wu, X.; Kollman, P. A. Amber 14 **2014**.

[27] Wang, J.; Wolf, R. M.; Caldwell, J. W.; Kollman, P. A.; Case, D. A. Development and testing of a general amber force field. *J. Comput. Chem*. **2004**, *25* (9), 1157-1174.

[28] Li, Y.; Liu, D.; Wang, P.; Zhou, Z. Computational Study of Enantioseparation by Amylose tris(3,5-dimethylphenylcarbamate)-based Chiral Stationary Phase. *J. Sep. Sci*. **2010**, *33*, 3245–3255.

[29] K. Sembongi, M. Tanaka, K. Sakurada, M. Kobayashi, S. Itagaki, T. Hirano and K. Iseki, A New Method for Determination of Both Thalidomide Enantiomers Using HPLC Systems. *Biol. Pharm. Bull*. **2008**, *31*, 497-500. PMID: 18310917

[30] Cirilli, R.; Ferretti, R.; De Santis, E.; Gallinella, B.; Zanitti, L.; La Torre, F. High Performance Liquid Chromatography Separation of Enantiomers of Flavanone and 2′-Hydroxychalcone Under Reversed-Phase Conditions. *J. Chromatogr. A* **2008**, *1190*, 95-101 (2008). DOI: 10.1016/j.chroma.2008.02.101

[31] J. S. Kang and G. Hempel, Effects of Diethylamine on Capillary Chromatographic Enantioseparation of Some Chiral Analytes Using Polysaccharide Stationary Phases with Pure Polar Solvents as Mobile Phases. *Bull. Korean Chem. Soc*. **2007**, *28*(6), 1035-1038. https://doi.org/10.5012/bkcs.2007.28.6.1035

[32] B. Chankvetadze, I. Kartozia, C. Yamamoto and Y. Okamoto, Comparative Enantioseparation of Selected Chiral Drugs on Four Different Polysaccharide Type Chiral Stationary Phases Using Polar Organic Mobile Phases. *J. Pharm. Biomed. Anal*. **2002**, *27*, 467-478.